



Observations and Numerical Simulation of Upper Boundary Layer Rapid Drying and Moistening Events during the International H₂O Project (IHOP_2002)

ROBIN L. TANAMACHI

School of Meteorology, University of Oklahoma, Norman, Oklahoma

WAYNE F. FELTZ

Cooperative Institute for Meteorological Satellite Studies, University of Wisconsin—Madison, Madison, Wisconsin

MING XUE

Center for Analysis and Prediction of Storms, and School of Meteorology, University of Oklahoma, Norman, Oklahoma

(Manuscript received 20 March 2007, in final form 9 January 2008)

ABSTRACT

On the morning of 12 June 2002, a series of upper boundary layer (UBL) rapid drying and moistening events (RDEs and RMEs, respectively) occurred at the “Homestead” site of the International H₂O Project (IHOP_2002). Over a period of 10 h, atmospheric water vapor in the UBL decreased or increased within a matter of minutes four separate times. High-temporal-resolution data of the RDEs and RMEs collected by numerous instruments deployed for this intensive observation period are presented. The results of an Advanced Regional Prediction System (ARPS) simulation of the weather conditions around the time period reproduced one of the two RDE–RME pairs with reasonably accurate amplitude and timing. Both the observational data and ARPS numerical model output indicate that the second RDE–RME pair resulted from the interaction between a dry air mass descending from the Rocky Mountains and a cold pool–internal undular bore couplet propagating over the Homestead site from a mesoscale convective complex to the north. The RDEs and RMEs, which were rarely observed during IHOP_2002, are believed to be an indirect indicator of such bores.

1. Introduction

During the intensive observation period (IOP) from 13 May to 25 June 2002 of the International H₂O Project (IHOP_2002), a large array of in situ, mobile, and aircraft-mounted water vapor sensing instruments from many institutions took collaborative water vapor measurements over the central United States (Weckwerth et al. 2004; Weckwerth and Parsons 2006). One of the specified objectives of IHOP_2002 was “improved characterization of the four-dimensional (4-D) distribution of water vapor and its application to improving the understanding and prediction of convection.” Owing to the intensive nature of the observation period, it

was also possible to investigate the converse in some detail.

It has long been known that convective systems can generate “cold pools” that can propagate like a density current or gravity current across the surface (Bluestein 1993, p. 441; Houze 1993, p. 477; Koch and Clark 1999). The passage of the gust front at the leading edge of this cold pool is often characterized by a pressure jump and wind shift. Under stably stratified conditions, a bore (Simpson 1987) may also develop and propagate above and ahead of the gust front. A bore is defined as a nonlinear vertical oscillation in a fluid associated with a horizontal discontinuity in fluid velocity. Internal bores (occurring in a stratified fluid) can produce smooth, nonturbulent waves that form and propagate at or slightly downstream of the location of the discontinuity, and these are known as “undular” bores (Simpson 1987). An observer may experience alternating pressure rises and falls as the “ripples” of such a bore pass

Corresponding author address: Robin Tanamachi, School of Meteorology, University of Oklahoma, 120 David L. Boren Blvd., Suite 5900, Norman, OK 73072-7307.
E-mail: rtanamachi@ou.edu

TABLE 1. Summary of RDE–RMEs A–D depicted in Fig. 1.

RDE–RME	Time (approx)	Relative changes above 250 m AGL	Relative changes near surface
A	0600 UTC	Drying, warming, decreased aerosols	Moistening, cooling, little wind shift
B	1000 UTC	Moistening, cooling, increased aerosols	Drying, warming, wind shift from southerly to northerly
C	1300 UTC	Drying, warming, decreased aerosols	Moistening, cooling wind shift from northerly to southerly
D	1600 UTC	Moistening, cooling, increased aerosols	Drying, warming, gradual wind shift from southerly to northwesterly

by overhead. At an observation point above the surface, the properties of the air may alternate between two states—with different temperatures, humidities, or wind speeds and directions—as the bore passes. A number of undular bores observed during IHOP are documented by Koch et al. (2003, 2005, 2008). Bores generally contain regions of rising and sinking air, and can potentially serve as convective triggers (Koch et al. 1991; Koch and Clark 1999).

As a propagating density current decays and decreases in depth and strength, the associated bore may transition to a solitary wave or a wave packet with multiple crests (Christie et al. 1978; Christie 1989; Knupp 2006). Solitary wave passage has been associated with a perturbation in observed surface pressure, which tends to return to the original value after passage (e.g., Doviak and Ge 1984; Fulton et al. 1990; Knupp 2006). Observational studies of transitions between bore and solitary wave phases are given by Fulton et al. (1990), Koch et al. (2005), Knupp (2006), and Koch et al. (2008).

Herein, we describe the occurrence of four upper boundary layer (UBL) rapid drying and moistening events (RDEs and RMEs, respectively) that occurred during the IHOP_2002 intensive observation period, on the morning of 12 June 2002 (Table 1). Several IHOP_2002 instruments at the “Homestead” site near Balko, Oklahoma (in the Oklahoma Panhandle), collected data during these events. The RDE–RMEs (denoted A–D) are best illustrated by the time–height plot of water vapor profiles measured by the Atmospheric Emitted Radiance Interferometer (AERI; Fig. 1; Feltz et al. 2003a,b; Knuteson et al. 2004a,b). High-resolution numerical simulations are performed for this event using the nonhydrostatic Advanced Regional Prediction System (ARPS) model (Xue et al. 2000, 2001, 2003). The model reproduced one of the two UBL RDE–RME pairs with reasonably accurate amplitude and timing. It is suggested that these RDE–RMEs were an indirect product of a nearby bore that was in the process of transitioning to a solitary wave packet.

The synoptic environment around the time of the RDE–RMEs is described in section 2. A description of

data collected during these events is given in section 3. The ARPS numerical simulation of these events is described in section 4. Possible causes of the RDEs–RMEs are discussed in section 5. A summary and conclusions are then given in section 6.

2. Synoptic-scale environment of 12 June 2002

To convey a more complete sense of the atmospheric conditions under which the RDE–RMEs occurred, we briefly discuss the synoptic-scale environment in the region of the Homestead site. At 0000 UTC 12 June 2002, a weak upper-level jet maximum (not shown) extended from eastern Wyoming to western Nebraska. An area of relatively high velocities at 300 hPa stretching southward into Colorado produced an upper-level region of decreasing (toward the east) wind speeds across the Oklahoma Panhandle. Atmospheric soundings from Dodge City, Kansas, and Amarillo, Texas, at 0000 UTC (Fig. 2) indicate that the atmospheric boundary layer was well mixed (with dry adiabatic temperature and constant water vapor profiles in at least the lowest 200 hPa) and neutrally stratified at both sites. The westerly winds aloft were stronger at Dodge City than at Amarillo, while the surface winds were southwesterly at Dodge City and southerly at Amarillo.

Infrared satellite imagery (Fig. 3) shows that two mesoscale convective systems (MCS1 and MCS2) moved from west to east across Kansas and into Missouri during the early morning hours of 12 June. Both systems produced strong outflow boundaries that passed over the Homestead site. Unfortunately for the purposes of this study, the S-Pol radar, located just west of the Homestead site, was not operational from 0000 to 1300 UTC 12 June. As a result, the exact time of the boundary passages over the Homestead site is not known, and must be estimated from data from more distant radars.¹

¹ An area of reflectivity detected by the S-Pol radar east of that radar site at around 1400 UTC (not shown) appeared to be too strong to be the outflow boundary from earlier convection and was almost certainly the second trip echo from MCS2, which by then was located east of Wichita, Kansas.

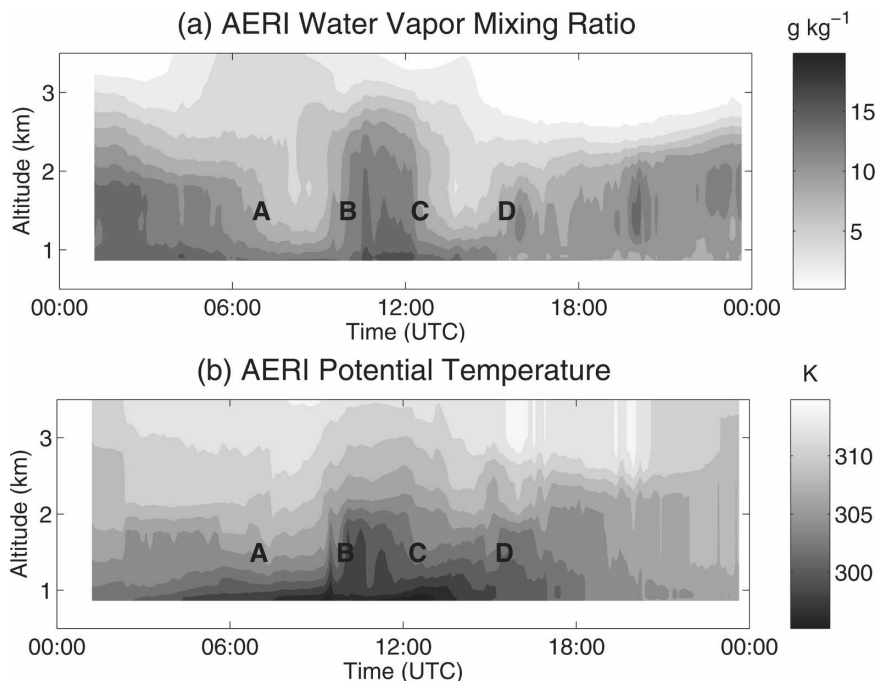


FIG. 1. Time–height plots of atmospheric water vapor mixing ratio (top; g kg^{-1}) and potential temperature (bottom; K) time series as a function of height over the Homestead site on 12 Jun 2002, using data retrieved from AERI measurements. The starting times of the four UBL RDE–RMEs are labeled A–D.

Animation of radar imagery taken by the Dodge City operational Weather Surveillance Radar-1988 Doppler (WSR-88D) in the outflow boundary from MCS1 revealed multiple ripples in the vicinity of the outflow boundary, an indication that this gust front was probably associated with an undular bore. This boundary weakened in intensity as it propagated south and west from MCS1, but it is believed to have reached the Homestead site around 0800 UTC, approximately 1 h after RDE A. As will be seen in section 3, this boundary was so weak as to be barely detectable in surface observations at the time it passed the Homestead site.

At 0816 UTC, a second, southward-moving outflow boundary from MCS2 was apparent about 10 km south of Dodge City in WSR-88D imagery (Fig. 4). From an isochronal analysis of the observed surface wind shift (from southerly to northerly winds) and pressure jump line associated with the outflow boundary (Fig. 5), the speed of the outflow boundary as it approached the Homestead site (between 1100 and 1400 UTC) was approximately 11 m s^{-1} . This figure is within 10% of the theoretical speed of a density current with a 6-K difference of potential temperature (θ) and a depth of 250 m (quantities derived from the AERI θ data, Fig. 1, to be further discussed in the next section; Bluestein 1993,

353–356). This outflow boundary passed over the Homestead site at approximately 1400 UTC.

3. Event description and data

Unless otherwise noted, all the instruments discussed in this section were located at the IHOP_2002 Homestead site near Balco, Oklahoma.

a. Atmospheric Emitted Radiance Interferometer data

According to Knuteson et al. (2004a), “the AERI instrument is a ground-based Fourier transform spectrometer for the measurement of accurately calibrated downwelling infrared thermal emission from the atmosphere.” The downwelling longwave infrared (3.3–19 μm) radiances, combined with supplemental Rapid Update Cycle (RUC) numerical weather prediction model-generated profiles, were used to infer temperature and moisture profiles in the atmospheric column above the instrument. The reader is referred to Feltz et al. (2003b) and Knuteson et al. (2004a,b) for a detailed description of the AERI instrument design and performance.

During IHOP_2002, temperature and water vapor

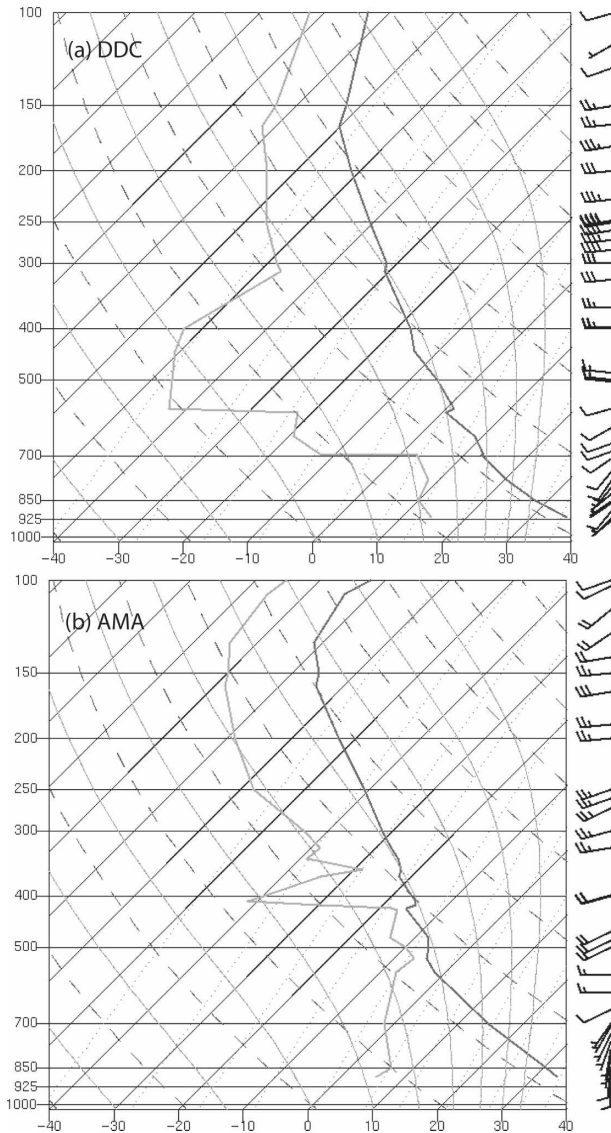


FIG. 2. Atmospheric soundings from (a) Dodge City, KS, and (b) Amarillo, TX, at 0000 UTC 12 Jun 2002. Source: UCAR JOSS IHOP_2002 catalog.

profiles were derived from radiance data in near-real time (Feltz et al. 2003a).² The derived atmospheric water vapor mixing ratio (q_v) and θ profiles from 12 June 2002 are found in Fig. 1. A stably stratified boundary layer extending up to approximately 1 km was overlaid by a deep, nearly neutrally stratified layer. The time

² A scanning Raman lidar (SRL) was also present at the Homestead site (Whiteman et al. 2006), and provided temperature and moisture profiles contemporaneous to those measured by the AERI. Unfortunately, the SRL was not operating during this time period.

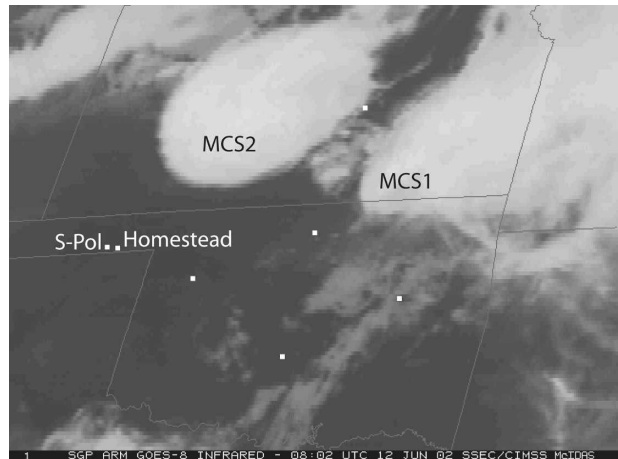


FIG. 3. GOES-8 infrared satellite imagery from 0802 UTC 12 Jun 2002. The two MCSs propagating to the east through KS are labeled MCS1 and MCS2. IHOP_2002 locations of the Homestead site and S-Pol radar (not operational at this time) are labeled; other white dots indicate locations of ARM program observation stations. Image courtesy of Space Science and Engineering Center (SSEC), University of Wisconsin—Madison.

series of q_v profiles exhibit a striking sequence of water vapor variations above about 250 m AGL. Four rapid UBL RDEs—RMEs (labeled A–D in Fig. 1) occurred between 0630 and 1700 UTC, with bottom to peak mixing ratio changes of ± 8 – 10 g kg^{-1} . The UBL RDEs—RMEs were separated by intervals of relatively constant q_v conditions lasting from 3 to 4 h. The UBL RDEs—RMEs were accompanied by fluctuations in θ on the order of ± 5 – 8 K , with warming associated with drying and cooling associated with moistening.

Near the surface, opposing fluctuations occurred in the q_v and θ , but with smaller amplitudes (± 2 – 5 g kg^{-1} and ± 1 – 5 K , respectively). These fluctuations were only vaguely indicative of the larger fluctuations occurring hundreds of meters above the surface. Bore passage is generally not associated with strong surface cooling (Koch and Clark 1999; Smith 1988).

b. Holographic Rotating Airborne Lidar Instrument Experiment (HARLIE) and Frequency Modulated Continuous Wave (FMCW) radar profiler data

The Holographic Rotating Airborne Lidar Instrument Experiment (HARLIE) is a conically scanning, $1\text{-}\mu\text{m}$ wavelength (infrared) lidar used to obtain high-resolution (30 m) profiles of relative aerosol backscatter coefficient (in arbitrary units) in the boundary layer (Schwemmer 1998). HARLIE data collected on 12 June 2002 (Fig. 6a) show a deep (up to 3 km AGL) layer of relatively high aerosol backscatter prior to A, a

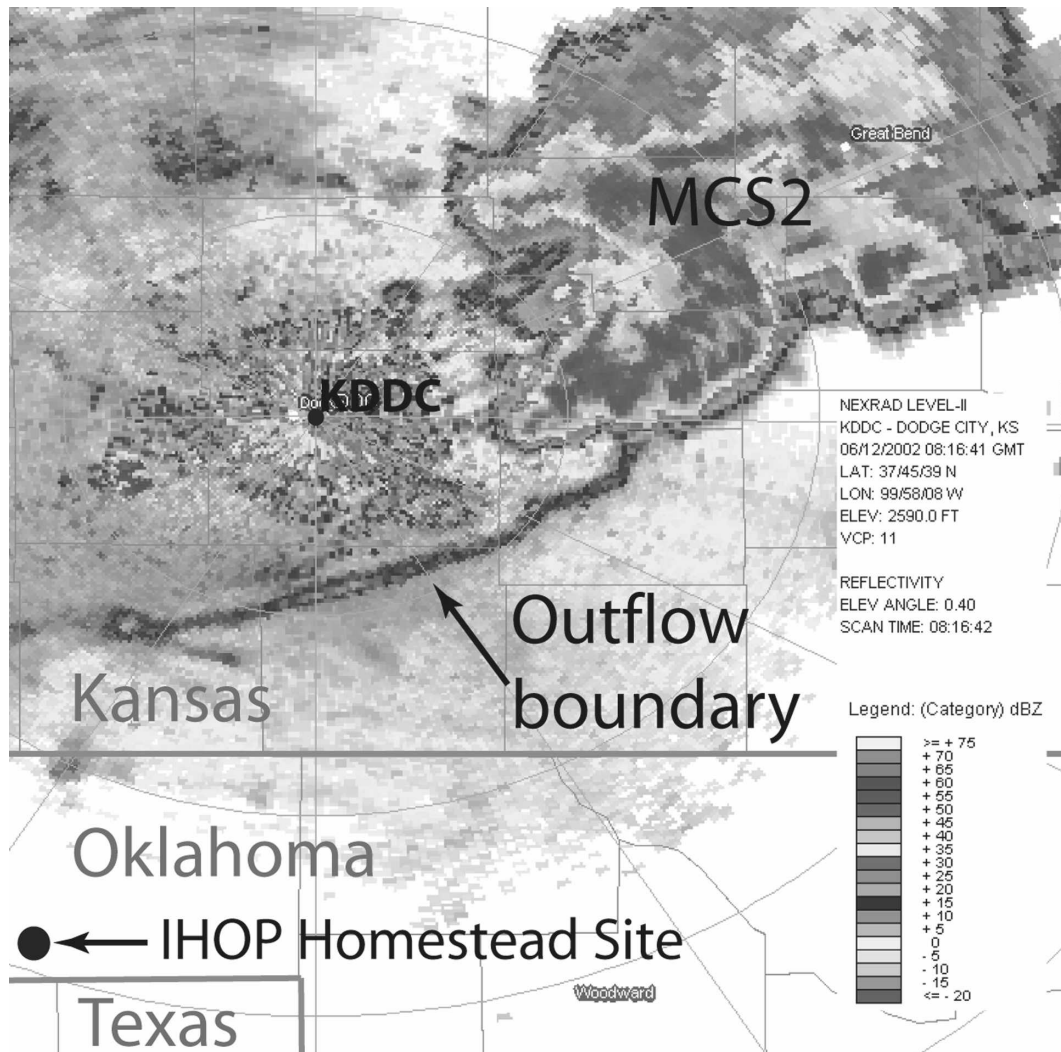


FIG. 4. Radar reflectivity (dBZ) image from the Dodge City, KS, WSR-88D (KDDC) radar at 0816 UTC 12 Jun 2002. Note the outflow boundary south of the KDDC radar site. The radar elevation angle was 0.4° ; range rings are 50 km apart. The Homestead site is denoted by the dot in the Oklahoma Panhandle. Data courtesy of NCDC.

rapid decrease in aerosols near and after A, a rapid increase near and after B, a decrease after C, and a final increase near D.

The University of Massachusetts (UMass) Frequency Modulated Continuous Wave (FMCW) radar profiler (Frasier et al. 2002) was used to profile aerosols in the atmospheric boundary layer over the Homestead site during IHOP_2002. The UMass FMCW radar is an S-band (2.9 GHz), pulse-compressed, dual-antenna system that furnishes very high-resolution (~ 2.5 m) reflectivity and velocity profiles of aerosol backscatter in the boundary layer directly above the radar. The top of the atmospheric boundary layer is usually indicated by a layer of relatively high vertical gradient in aerosol backscatter.

The HARLIE data can be interpreted as a combined aerosol–humidity indicator, and the UMass FMCW data are predominantly aerosol indicative. The aerosol profiles collected by the UMass FMCW radar on 12 June 2002 (Fig. 6b) show a good agreement with those from the HARLIE (Fig. 6a); both exhibit relatively high concentrations of aerosols in a wavelike pattern over the Homestead site with a periodicity approximately matching that of the RDE–RMEs (from 3 to 4 h). The primary differences between the two fields likely result from the different wavelengths and units being used. In general, UBL RDEs (RMEs) were associated with decreases (increases) in atmospheric aerosol backscatter coefficient and decreases (increases) in the height of the top of the boundary layer.

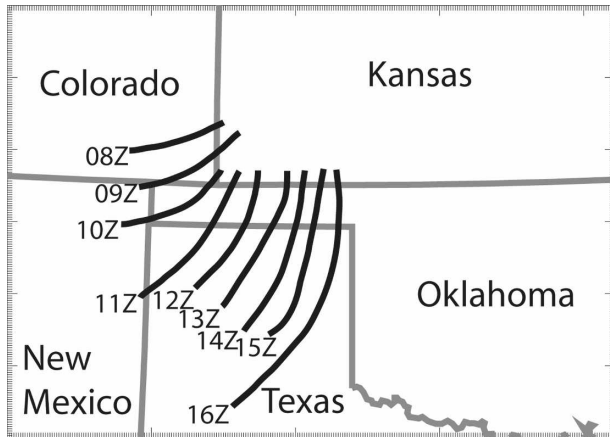


FIG. 5. Isochronal analysis from surface observations of the wind shift line associated with the outflow boundary from MCS2 (Fig. 3), as it moved south and east across the Oklahoma Panhandle from 0800 to 1600 UTC 12 Jun 2002.

In particular, around the time of RDE A (C), the height of the top of the boundary layer decreased by 1150 m (1000 m); the corresponding decrease in height for RME B (D) was 1100 m (600 m; Fig. 6b). These measurements appear to corroborate the idea that bound-

ary layer air (along with aerosols) was transported up and down over the Homestead site as a result of the bore/solitary wave passage.

c. Multiple Antenna Profiler

The Multiple Antenna Profiler (MAPR) is a 33-cm wavelength, skyward-pointing Doppler radar designed to rapidly measure vertical velocity in the boundary layer (Cohn et al. 2001). The MAPR vertical velocity profiles above the Homestead site on 12 June 2002 (Fig. 7a) show that vertical velocity in the UBL briefly decreased to -0.5 m s^{-1} about 30 min before RDE A, and then increased to 1 m s^{-1} for a period of between 30 and 60 min about 30 min prior to RME B. These vertical velocity profiles are consistent with the passage of a bore (e.g., Koch et al. 2003, see their Fig. 4b). However, no appreciable change in UBL vertical velocity was associated with RDE C or RME D, suggesting that the structure may have been less borelike at this stage of the passage.

From the MAPR data, vertical displacement of the top of the boundary layer around the time of RME B was predicted using the technique of Koch and Clark (1999). In this technique, the spatial pattern of vertical

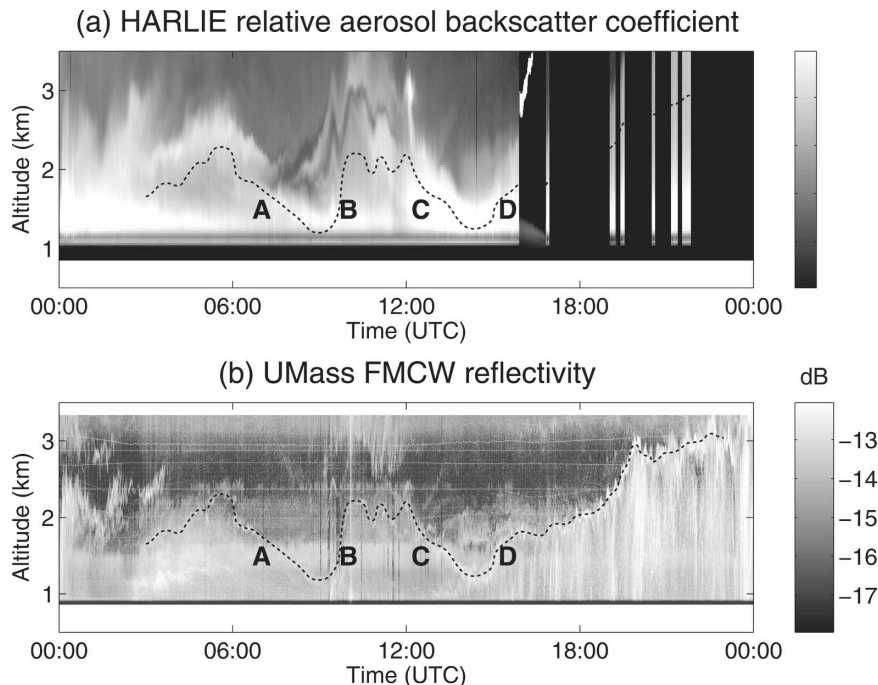


FIG. 6. Time–height plots of (a) HARLIE relative aerosol backscatter coefficient (arbitrary units) and (b) UMass FMCW reflectivity (dB) in the boundary layer of the Homestead site on 12 Jun 2002. The dashed curve in (b) highlights a layer of relatively high reflectivity (used as a proxy for the top of the boundary layer) around the time of the RDE–RMEs; this curve is reproduced in (a) for ease of comparison.

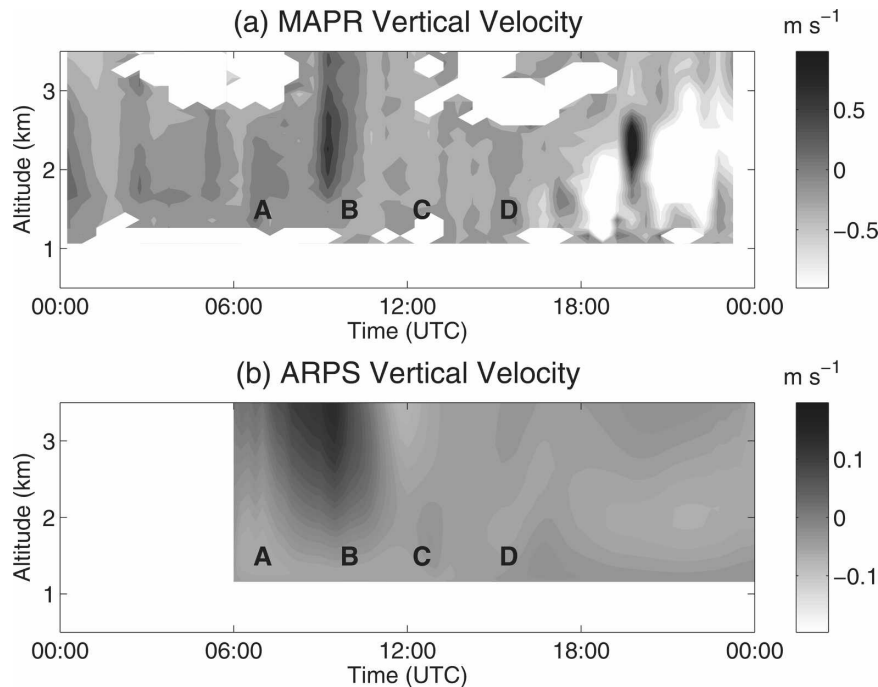


FIG. 7. Time–height plots of vertical velocity (m s^{-1}) over the Homestead site (a) as measured by the MAPR and (b) as simulated by the ARPS at 3-km horizontal resolution (discussed later). Note that the gray shading scales differ between (a) and (b).

velocity pattern of the bore passage was modeled as a simple cosine function, and vertical displacement was estimated by temporal integration of this function. The resultant estimate of the maximum vertical displacement of the top of the boundary layer was 1260 m, greater than the observed increase (Fig. 6b) of 1100 m. At the time of passage, the bore appeared to be in transition to a slightly less vigorous solitary wave, which may explain the discrepancy between the calculated vertical displacement and the observed.

d. Surface data

A National Center for Atmospheric Research (NCAR) Integrated Sounding System (ISS) automated weather station at the Homestead site recorded thermodynamic and wind measurements throughout the IHOP_2002 deployment. The measurements from the morning of 12 June 2002 exhibit some sharp transitions around the time of some of the RDE–RMEs, but not all (Fig. 8). Prior to the RDE–RMEs, the sky conditions over the Homestead site were clear with southerly winds. RDE A was associated with a gradual decrease in surface pressure and temperature. RME B was associated with an increase in pressure from 908 to 911 hPa. Christie et al. (1978) simulated surface pressure traces associated with the passage of wave packets and solitary waves; the Homestead pressure trace near the

time of RDE A and RME B superficially resembles that associated with the passage of a solitary wave of depression. Knupp (2006) reported that a bore passage (supported by a trailing density current) is associated with the surface pressure increase that persists long after the passage. In contrast, the passage of a solitary wave is associated with a surface pressure increase that subsequently shrinks until the surface pressure returns to near its original value. In the present case, the pressure trace appears to show a pressure perturbation (such as that associated with the passage of a solitary wave of depression) superimposed upon an overall pressure rise (like that associated with a bore passage). This pressure trace suggests that the bore may have been transitioning to a solitary wave at the time that the pressure trace was recorded. A similar pressure trace was documented by Knupp (2006; see their Fig. 7) in the wake of a bore passage.

RME B was associated with a relatively dramatic wind shift pattern at the surface: the wind direction switched from southerly to northerly and then slowly returned to a southerly direction via a series of smaller-scale oscillations (Fig. 8e). It can be inferred from these oscillations that the outflow feature passing over the Homestead site retained some borelike features. Koch and Clark (1999) stipulated that a bore passage would be preceded by a region of surface flow in the opposite

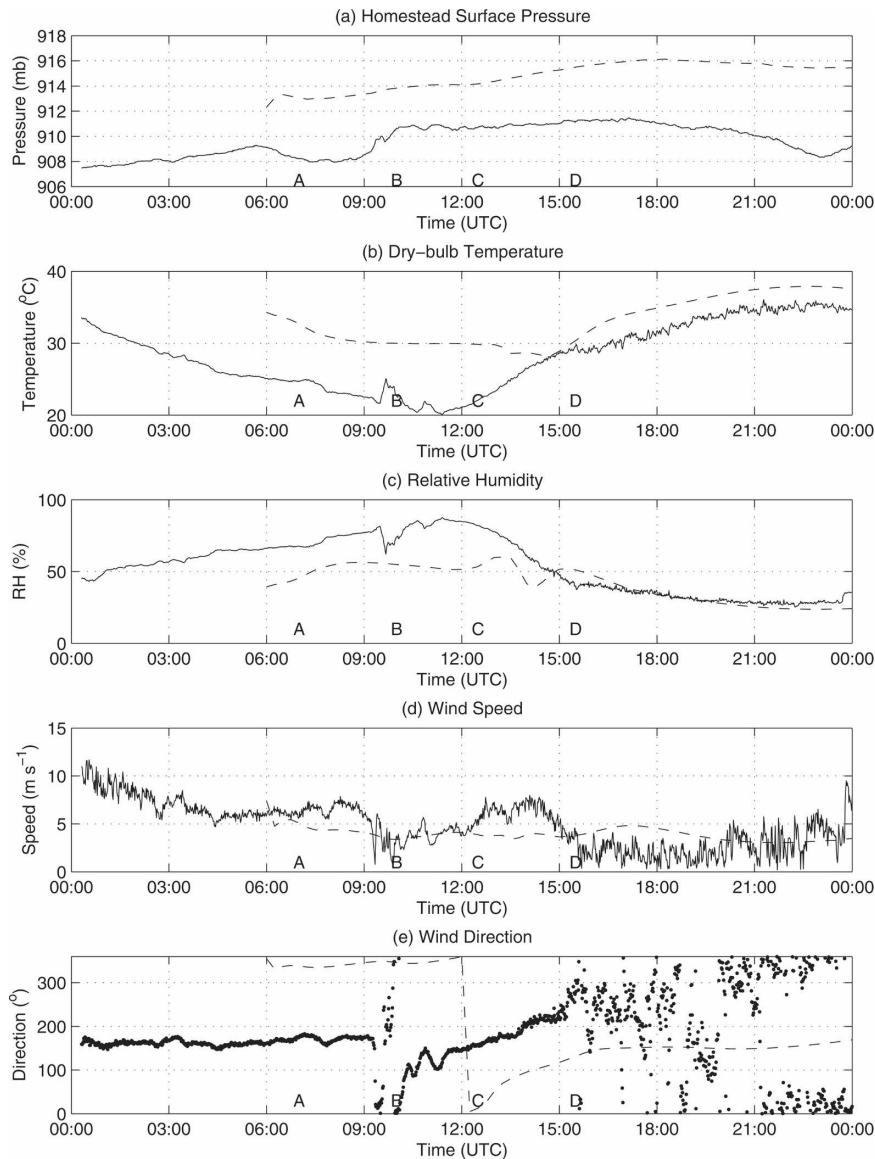


FIG. 8. Homestead observed (solid curves) and 3-km horizontal resolution ARPS simulated (dashed curves, discussed later) surface (a) pressure (hPa), (b) temperature (°C), (c) relative humidity (%), (d) wind speed (m s⁻¹), and (e) wind direction (° clockwise from north).

direction to the bore's propagation. Knupp (2006) refers to this flow as a component of the convergent boundary zone (CBZ). The surface wind measurements show that the surface flow did indeed turn from southerly to northerly immediately prior to RME B.

RME D signaled the onset of relatively quiescent surface winds that persisted through the remainder of the period of study. It is believed that the departure of MCS2 from the area of the Homestead site and the associated removal of the cold outflow source resulted in relatively calm winds following the bore/solitary wave passage.

4. ARPS simulations

Despite the availability of high-frequency observations of boundary layer profiles of moisture and temperature, a complete picture of the processes responsible for the RDE-RMEs is still difficult to infer from the observational data alone. Most of the observed characteristics were reproduced in a high-resolution numerical model simulation, making a complete three-dimensional simulated dataset available for detailed analysis. For this case study, a set of nested grid numerical simulations of the atmosphere over the Home-

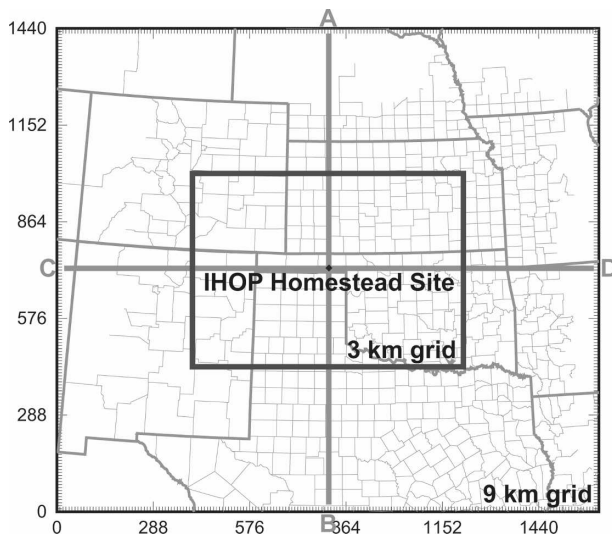


FIG. 9. The ARPS 9- and 3-km-resolution computational domains used in this study. Axes labels are in kilometers from the lower-left corner of the 9-km grid. The lines labeled A–B and C–D are the locations of cross sections (discussed later).

stead site were performed using the Advanced Regional Prediction System (ARPS) model developed at the Center for Analysis and Prediction of Storms (CAPS) at the University of Oklahoma (OU). A detailed description of the model and its applications can be found in Xue et al. (2000, 2001, 2003).

ARPS was used because real-time, high-resolution numerical predictions were performed as part of the forecasting component of IHOP_2002 (Xue et al. 2002); the datasets gathered in real time as part of IHOP_2002 enabled easy application of the model to this study. Subsequently, ARPS has been used to perform detailed data assimilation and simulation studies for several IHOP_2002 cases (Xue and Martin 2006; Dawson and Xue 2006; Liu and Xue 2008) and excellent agreement between the simulations and observations were obtained in these studies. In fact, Liu and Xue (2008) studied the convective initiation processes of 12 June 2002, although the model was initialized at 1200 UTC and performed hourly data assimilation cycles through 1800 UTC. Convective initiation was well captured along the dryline in the Texas Panhandle about 2 h after 1800 UTC.

In the ARPS simulations of this study, two different domains were utilized (Fig. 9). The first was a 9-km-resolution grid covering most of the central plains and centered exactly on the Homestead site (36.56°N, 100.61°W). The second domain was a one-way nested 3-km-resolution grid centered at the same location. The grid sizes used were $163 \times 183 \times 53$ and $273 \times 195 \times 53$, respectively. The configurations of these two grids

closely follow those of the corresponding grids used in the CAPS real-time experiment (Xue et al. 2002). Both grids used 53 vertical levels with the top of the model domain at 20 km above sea level. The vertical resolution ranged from about 20 m at the surface to nearly 800 m at the top. The first scalar level, where all atmospheric state variables except for vertical velocity are defined, was about 10 m above ground. The ARPS physics packages employed included the three-ice Lin et al. (1983) microphysics scheme, a new version of the Kain–Fritsch cumulus parameterization scheme (on the 9-km grid only), long- and shortwave radiation parameterization including cloud interactions, 1.5-order TKE-based three-dimensional subgrid-scale turbulence and TKE-based PBL parameterizations, stability-dependent surface layer physics, and a two-layer soil model. In addition, a fourth-order centered difference advection scheme was used [more details can be found in Xue et al. (2000), (2001), and (2003)]. Three-second-resolution topographical data and 1-km-resolution land surface characteristics data were used to define the land surface characteristics in the soil–vegetation model.

The ARPS Data Analysis System (ADAS; Brewster 1996) was used to create high-resolution analysis using routine as well as special observations, including those of regional mesoscale networks, on the 9-km grid. The analysis was performed for 0600 UTC using the 6-h forecast from the 0000 UTC cycle of the operational NCEP Eta Model as the background. The special data used include

- surface observations from the Oklahoma, southwest Kansas, and west Texas Mesonets,
- the Atmospheric Radiation Measurement (ARM) Program Surface Meteorological Observation System (SMOS) data,
- Big Bend (Kansas) groundwater Management District Number 5 soil and surface observations, and
- aircraft-borne Meteorological Data Collection and Reporting System (MDCRS) observations.

A more detailed description of these data can be found in Dawson and Xue (2006, see their Table 1). The configurations of ADAS were also similar to those of Dawson and Xue (2006), except that radar data were not used in this study. Inclusion of the special surface data enabled the ADAS to capture the effects of the ongoing MCSs and their associated outflow boundaries at model initialization. Inclusion of MDCRS data provided boundary layer soundings at nearby airports as well as upper-air information at nonsynoptic times.

Both the 9- and 3-km runs were initialized at 0600 UTC 12 June 2002, approximately 1 h prior to RDE A. The 9-km forecast was first run for 18 h (to 0000 UTC

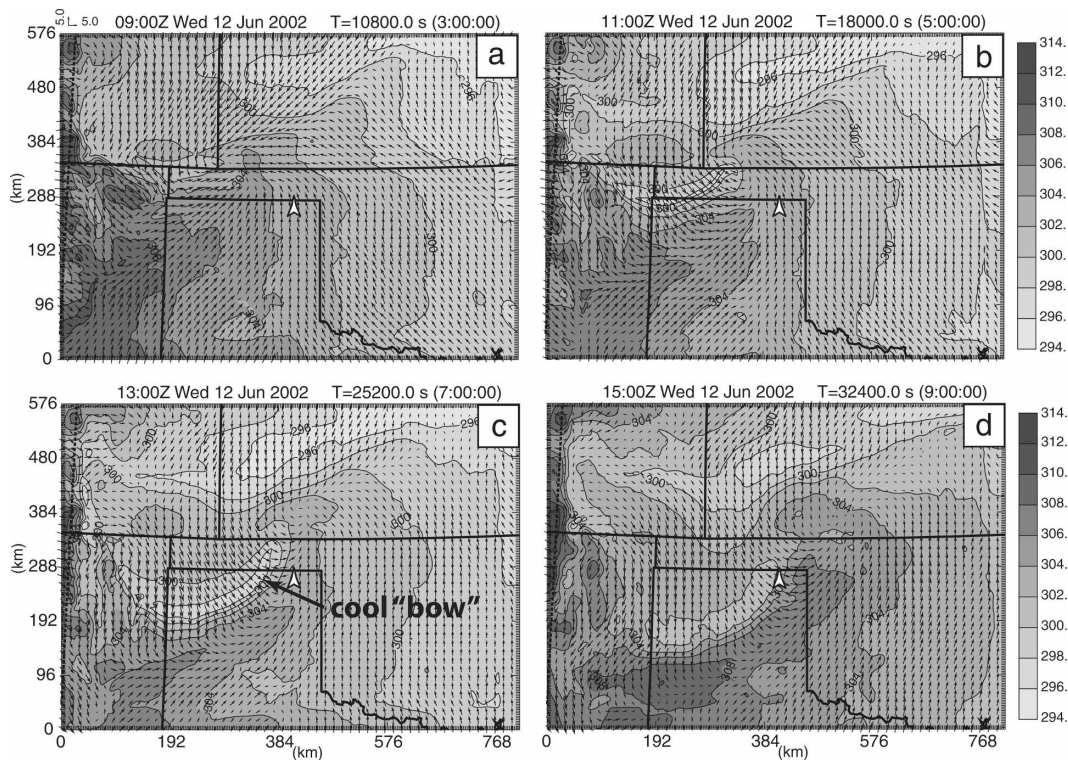


FIG. 10. ARPS simulated surface potential temperature (K) fields on the 3-km grid at (a) 0900, (b) 1100, (c) 1300, and (d) 1500 UTC 12 Jun 2002. The tip of the white arrowhead denotes the location of the IHOP_2002 Homestead site.

13 June 2002), using the 6-h Eta forecasts from the 0000 UTC cycle as the boundary conditions. The 3-km run was initialized from the interpolated 9-km ADAS analysis and forced at the lateral boundaries by the 9-km ARPS forecasts. The 3-km forecast was also run to 0000 UTC 13 June 2002.

5. Simulation results

From the plots of ARPS surface θ fields from the 3-km simulation (Fig. 10), it can be seen that a bow-shaped region of relatively low θ propagates over the Homestead site. The bow of relatively low θ initially forms at around 0900 UTC along a wind shift line in southwest Kansas, which is the leading edge of the outflow from MCS2 to the north, and it trails slightly behind the wind shift line by 5–10 km for the duration of its existence. It propagates to the southeast (into the Oklahoma and Texas Panhandles) at a velocity of approximately 9 m s^{-1} , close to what would be expected for a density current with a 5° θ gradient across the gust front (Bluestein 1993), as found in the θ fields. This simulated feature is consistent with the observations of a wind shift line (Fig. 5) and surface θ decrease (Fig. 1) at the Homestead site.

A series of meridional cross sections (Fig. 11) through the longitude of the Homestead site in the 9-km run (line A–B in Fig. 9, the 9-km fields are shown here to include more of the interesting features) show a surface pool of low- θ air, approximately 750 m thick at its thickest point, propagating primarily from north to south in the northern portion of the ARPS domain, against the prevailing southerly winds. In this meridional cross section, the profile of this propagating cold pool strongly resembles that of a density current with a somewhat elevated head. Starting at 1100 UTC, ahead of the density current, a series of nonlinear, borelike waves in the θ contours can be seen, which are most intense at about the 3-km level, well above the top of the density current–like structure. The “bore intensity” (Koch et al. 2005), that is, the ratio between the simulated “bore” depth (about 3 km) and the pre-RDE A boundary layer depth (about 2 km; see Fig. 6b), is 1.5, a value corresponding to a “smooth, undular bore.” These waves propagated primarily from north to south, in the same direction as the leading edge of the density current. At 1500 UTC (Fig. 11d), the borelike feature in the isentropes is farther ahead of the density current than at earlier times (Fig. 11b), indicating that the waves are propagating at a faster speed than the leading

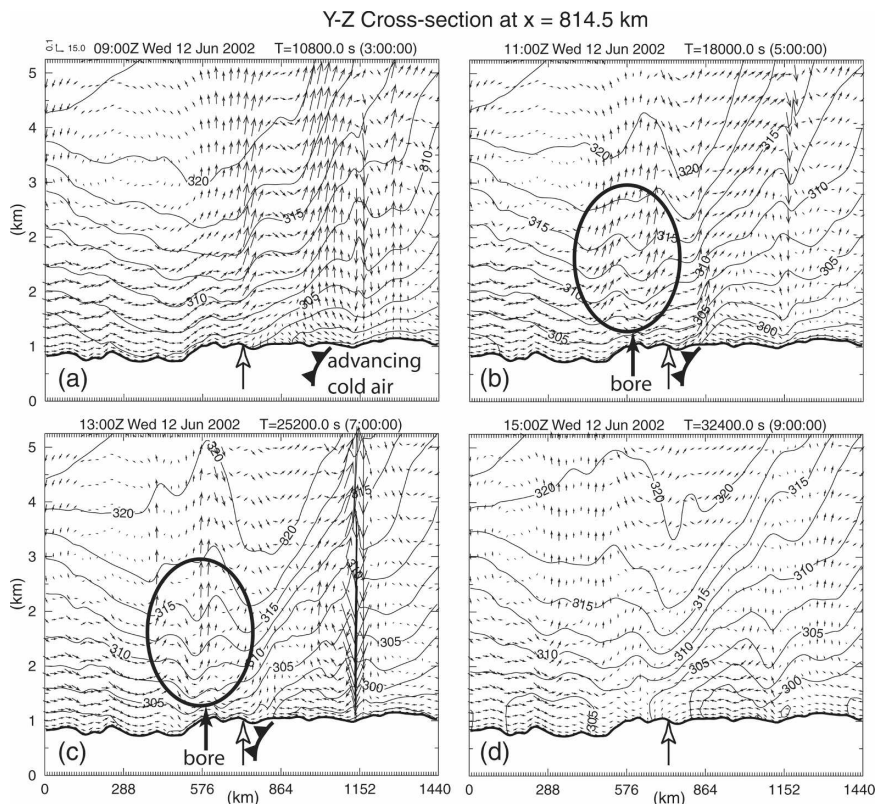


FIG. 11. Meridional cross section (at the longitude of the Homestead site: line A–B in Fig. 9) of 9-km-resolution ARPS-simulated potential temperature field (K) at (a) 0900, (b) 1100, (c) 1300, and (d) 1500 UTC 12 Jun 2002. North is toward the right edge of the page. The tip of the white arrowhead denotes the location of the IHOP_2002 Homestead site.

edge of the density current itself. These characteristics fit the conceptual model of a density current–atmospheric undular bore couplet as described by Simpson (1987) and the distinctive characteristics of a bore as described by Koch and Clark (1999).

A pronounced, eastward-propagating, downslope surge of very dry air can be seen in a series of both meridional (Fig. 12) and zonal cross sections of q_v (Fig. 13), and appears as a dryline at the surface. In these views, it can be seen that a dry air “wedge” becomes uncoupled from the surface around 1300 UTC owing to the intrusion from the north of cold outflow air, but it continues to propagate toward the east above a shallow layer of moist air. The dry air wedge passes the longitude of the Homestead site, but causes little change in the q_v at the surface. Here, θ and q_v isosurface analyses (not shown) illuminated the spatial relationship between these two features. The dry air wedge propagates just ahead of the leading edge of the low- θ air and behind the apparent bore. This motion results from the interaction of a dryline descending from the Rockies with the bore waves to its south, which has a strong

downward component of motion at that location. The downward motion in the bore serves to draw the wedge of dry air downward very quickly, but subsequent upward motion decouples the dry air from the surface just before it reaches the Homestead site.

The ARPS 3-km-resolution simulation shows upward motion around 1030 UTC at the grid point closest to the Homestead site (Fig. 8b), and this simulated maximum matches very closely the time and height AGL of that observed by the MAPR (Fig. 8a). However, the duration of the vertical velocity maximum is longer, and magnitude smaller (0.2 versus 1.0 m s^{-1} as observed by the MAPR) in the model. These differences likely arise from the still relatively coarse 3-km resolution used by the model, which may not be sufficiently high for small-scale details to be more quantitatively correct.

The ARPS-simulated profiles of q_v and θ over the Homestead site (Fig. 14) can be directly compared with the profiles recorded by the AERI (Fig. 1). RDE C and RME D are reproduced with reasonable amplitude and timing. Although the rapid cooling at the low levels is

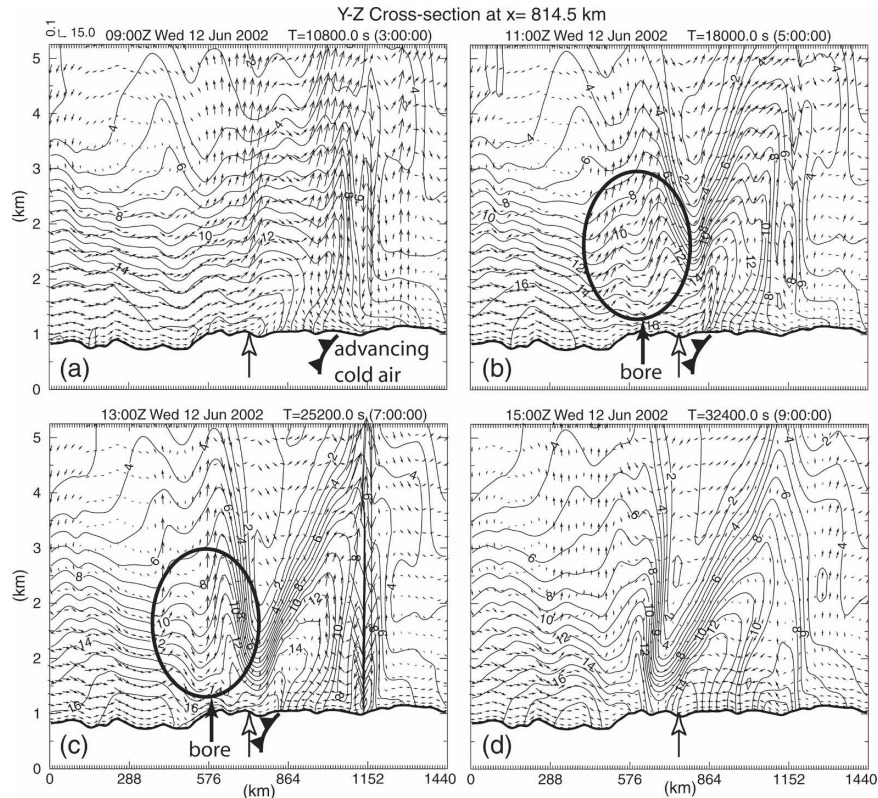


FIG. 12. As in Fig. 11, but for the simulated water vapor mixing ratio field. (b)–(d) Note the wedge of dry air (moving out of the page).

captured well in the model (Figs. 14b and 1b), RDE A and RME B do not appear in the simulations. In fact, RDE A (RME B) is simulated as a marginal moistening (drying) event detectable at the surface. The reasons for this discrepancy are unclear. An additional ARPS simulation was conducted that was identical to the present simulation except that it was initialized at 0000 UTC; similar simulation results in the 0600–1200 UTC time period indicated that the model “spinup” problem does not seem to be the primary cause of the absence of the first RDE–RME pair. We speculate that observed RDE A and RME B are related to the cold pool and gust front originating from the earlier MCS1 via a process similar to that which formed the second RDE–RME pair in the ARPS simulations. Because MCS1 was located farther away from the Homestead site, its cold pool and gust front diminished in strength by the time they reached the Homestead site, and more so in the model than in the observations. The relatively weak outflow boundary from MCS1 may not have been assimilated into the ARPS simulations with sufficient accuracy and resolution to result in a proper reproduction of any associated bore, and hence, of the first RDE–RME pair.

Using the ARPS simulation results as guidance, a conceptual model of the second pair of 12 June 2002 UBL RDE–RMEs was developed (Fig. 15). The ARPS simulation indicated that a descending dry air wedge from the Rockies interacted with a southward-propagating atmospheric undular bore (which may have been in the process of transitioning to a solitary wave) associated with the cold pool–gust front couplet produced by MCS2 in southwest Kansas (Fig. 15). The cold pool undercut the eastward-propagating dry air, while areas of rising and sinking motion associated with the bore served to decouple the dry air from the surface just west of the Homestead site and formed an eastward-propagating “dry wedge” slightly aloft. As a result, when the dry air wedge passed over the Homestead site, it registered in the AERI data above about 250 m but not below (also corroborated by surface measurements, which showed that the surface dryline never progressed any farther east than the Texas–New Mexico border). At the same time, relatively low- θ air in the MCS2 outflow was observed near the surface. This simulated wedge of dry air produced boundary layer moisture profiles similar to those seen in the AERI data.

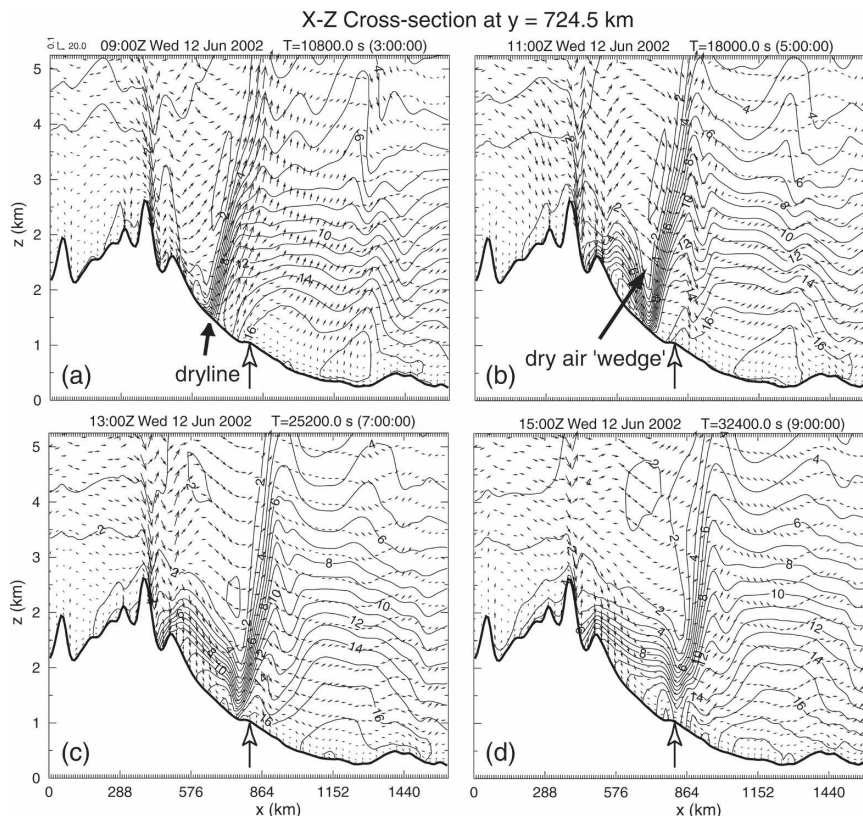


FIG. 13. Zonal cross section (at the latitude of the Homestead site: line C–D in Fig. 9) of 9-km-resolution ARPS-simulated water vapor mixing ratio (g kg^{-1}) field at (a) 0900, (b) 1100, (c) 1300, and (d) 1500 UTC 12 Jun 2002. The tip of the white arrowhead denotes the location of the IHOP_2002 Homestead site.

6. Conclusions

Two pairs of UBL RDE–RMEs were observed on the morning of 12 June 2002 over the IHOP_2002 Homestead site in the Oklahoma Panhandle. Data collected by multiple instruments at the Homestead site showed in great detail the timing and structure of the RDE–RMEs and attendant fluctuations in θ , atmospheric aerosols, and vertical velocity. It was speculated that the first RDE–RME pair was associated with the passage of the outflow boundary from a mesoscale convective complex (MCS1) in south central Kansas, while the later RDE–RME pair were associated with the stronger outflow boundary from another MCS (MCS2) in southwest Kansas.

The conditions of the RDE–RMEs were simulated using the ARPS model at 9- and 3km horizontal resolutions in a one-way nested mode. It can be seen that the simulation reproduced the later RDE–RME pair clearly, but the earlier RDE–RME pair was almost entirely absent (Fig. 14). The formation mechanisms of

the later RDE–RME pair were elucidated by the model solution and corroborated by the observations, and the information allowed for the construction of a conceptual model of the events (Fig. 15). It is suggested that the earlier RDE–RME pair formed via a process similar to that of the later pair, but was not reproduced clearly by the ARPS model for reasons that are not entirely clear. It is suspected that the MCS1 outflow boundary may have been too weak to be fully captured in the initial condition and simulation of the ARPS model; the model therefore failed to reproduce the associated bore. Future simulation studies with increased resolution and improved data assimilation, perhaps including radar data through assimilation cycles, might be able to reproduce the first RDE–RME pair.

To the best of the authors' knowledge, the data collected in the RDE–RMEs of 12 June 2002 are unique, and the phenomenon of such RDE–RMEs is either unknown or underreported. The relative abundance of data from IHOP_2002 made it possible to study the evolution of these events in great detail (e.g., Knupp

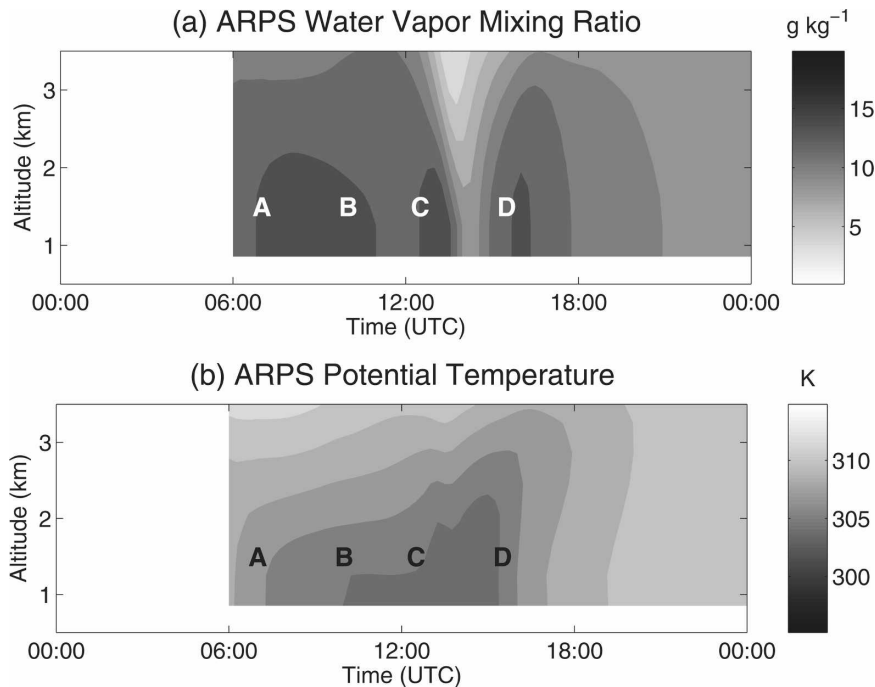


FIG. 14. Time series of (top) water vapor mixing ratio (g kg^{-1}) and (bottom) potential temperature, from 3-km-horizontal-resolution ARPS simulation of the IHOP_2002 domain, at the grid point closest to the Homestead site. (cf. Fig. 1).

2006, see his Fig. 8). In this study, the ARPS mesoscale model reproduced the later RDE–RME pair, lending confidence to our suggestion on the atmospheric processes responsible. While these RDE–RMEs were not directly associated with convective initiation, it has been documented that the vertical air motions associated with atmospheric undular bores can serve as convective triggers (Koch et al. 1991). Water vapor profiles from instruments such as the AERI could potentially indicate the presence of nearby bores before they trigger convection. Efforts toward the detection of such phenomena could prove useful in improving short-term forecasts of convection.

Acknowledgments. This research began as a class project of the first author. A majority of the Homestead data was supplied by the University Cooperation for Atmospheric Research (UCAR) Joint Office for Science Support (JOSS). The authors are grateful to Henry J. Neeman and the OU Supercomputing Center for Education and Research (OSCAR) for providing supercomputing resources. Daniel T. Dawson II provided guidance to the first author regarding the use of the ARPS model and interpretation of the results. Howard B. Bluestein and Steven E. Koch provided helpful discussion during the development of this manuscript. NSF Grant ATM-0129892 supported the CAPS real-time forecast during IHOP_2002 and sub-

sequent case studies together with Grant ATM-0530814. The authors also acknowledge the three anonymous reviewers of this manuscript, whose comments greatly improved its scope and clarity.

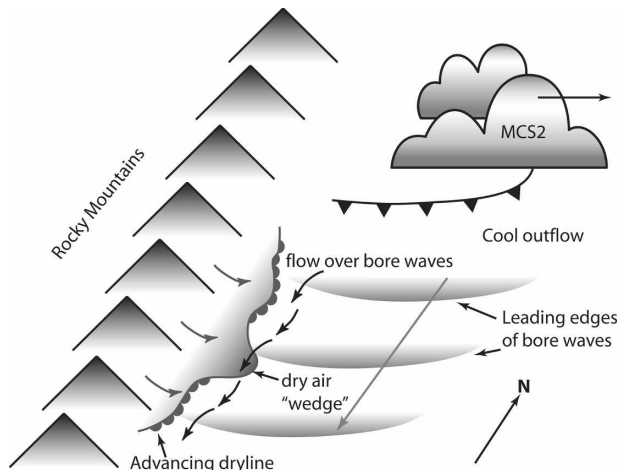


FIG. 15. A conceptual model of the interaction between the bore associated with the outflow from MCS2 and the advancing dryline that produced the wedge of dry air depicted in the ARPS model simulations. The southward-moving bore waves, with their attendant regions of rising and sinking motion, generate “kinks” in the advancing dryline and, in some locations, decouple the dryline from the surface. One of the downward kinks in the dryline is shaped into the wedge (Fig. 13) by continued interaction with the bore.

REFERENCES

- Bluestein, H. B., 1993: *Synoptic-Dynamic Meteorology in Mid-Latitudes. Volume II: Observation and Theory of Weather Systems*. Oxford University Press, 594 pp.
- Brewster, K., 1996: Application of a Bratseth analysis scheme including Doppler radar data. Preprints, *15th Conf. on Weather Analysis and Forecasting*, Norfolk, VA, Amer. Meteor. Soc., 92–95.
- Christie, D. R., 1989: Long nonlinear waves in the lower atmosphere. *J. Atmos. Sci.*, **46**, 1462–1490.
- , K. J. Muirhead, and A. L. Hales, 1978: On solitary waves in the lower atmosphere. *J. Atmos. Sci.*, **35**, 805–825.
- Cohn, S. A., W. O. J. Brown, C. L. Martin, M. E. Susedik, G. Maclean, and D. B. Parsons, 2001: Clear air boundary layer spaced antenna wind measurement with the Multiple Antenna Profiler (MAPR). *Ann. Geophys.*, **19**, 845–854.
- Dawson, D. T., II, and M. Xue, 2006: Numerical forecasts of the 15–16 June 2002 Southern Plains severe MCS: Impact of mesoscale data and cloud analysis. *Mon. Wea. Rev.*, **134**, 1607–1629.
- Doviak, R. J., and R. Ge, 1984: An atmospheric solitary gust observed with a Doppler radar, a tall tower, and a surface network. *J. Atmos. Sci.*, **41**, 2559–2573.
- Feltz, W. F., D. Posselt, J. Mecikalski, G. S. Wade, and T. J. Schmit, 2003a: Rapid boundary layer water vapor transitions. *Bull. Amer. Meteor. Soc.*, **84**, 29–30.
- , W. L. Smith, H. B. Howell, R. O. Knuteson, H. Woolf, and H. E. Revercomb, 2003b: Near-continuous profiling of temperature, moisture, and atmospheric stability using the Atmospheric Emitted Radiance Interferometer (AERI). *J. Appl. Meteor.*, **42**, 584–597.
- Frasier, S. J., T. Ince, and F. Lopez-Dekker, 2002: Performance of S-band FMCW radar for boundary layer observation. Preprints, *15th Conf. on Boundary Layer and Turbulence*, Wageningen, Netherlands, Amer. Meteor. Soc., 7.7. [Available online at <http://ams.confex.com/ams/pdfpapers/44067.pdf>.]
- Fulton, R., D. S. Zrnich, and R. J. Doviak, 1990: Initiation of a solitary wave family in the demise of a nocturnal thunderstorm density current. *J. Atmos. Sci.*, **47**, 319–337.
- Houze, R. A., 1993: *Cloud Dynamics*. Academic Press, 573 pp.
- Knupp, K., 2006: Observational analysis of a gust front to bore to solitary wave transition within an evolving nocturnal boundary layer. *J. Atmos. Sci.*, **63**, 2016–2035.
- Knuteson, R. O., and Coauthors, 2004a: Atmospheric Emitted Radiance Interferometer. Part I: Instrument design. *J. Atmos. Oceanic Technol.*, **21**, 1763–1776.
- , and Coauthors, 2004b: Atmospheric Emitted Radiance Interferometer. Part II: Instrument performance. *J. Atmos. Oceanic Technol.*, **21**, 1777–1789.
- Koch, S. E., and W. L. Clark, 1999: A non-classical cold front observed during COPS-91: Frontal structure and the process of storm initiation. *J. Atmos. Sci.*, **56**, 2862–2890.
- , P. B. Dorian, R. Ferrare, S. H. Melfi, W. C. Skillman, and D. Whiteman, 1991: Structure of an internal bore and dissipating gravity current as revealed by Raman Lidar. *Mon. Wea. Rev.*, **119**, 857–887.
- , and Coauthors, 2003: Structure and dynamics of a dual bore event during IHOP as revealed by remote sensing and numerical simulation. Preprints, *Sixth Int. Symp. on Tropospheric Profiling: Needs and Technologies*, Leipzig, Germany, Institute for Tropospheric Research, 378–380.
- , M. Pagowski, J. W. Wilson, F. Fabry, C. Flamant, W. Feltz, G. Schwemmer, and B. Geerts, 2005: The structure and dynamics of atmospheric bores and solitons as determined from remote sensing and modeling experiments during IHOP. Preprints, *32nd Conf. on Radar Meteorology*, Albuquerque, NM, Amer. Meteor. Soc., JP6J.4. [Available online at <http://ams.confex.com/ams/pdfpapers/97033.pdf>.]
- , W. F. Feltz, F. Fabry, M. Pagowski, B. Geerts, K. M. Bedka, D. O. Miller, and J. W. Wilson, 2008: Turbulent mixing processes in atmospheric bores and solitary waves deduced from profiling systems and numerical simulation. *Mon. Wea. Rev.*, **136**, 1373–1400.
- Lin, Y.-L., R. D. Farley, and H. D. Orville, 1983: Bulk parameterization of the snow field in a cloud model. *J. Climate Appl. Meteor.*, **22**, 1065–1092.
- Liu, H., and M. Xue, 2008: Prediction of convective initiation and storm evolution on 12 June 2002 during IHOP_2002. Part I: Control simulation and sensitivity experiments. *Mon. Wea. Rev.*, **136**, 2261–2282.
- Schwemmer, G. K., 1998: Holographic Airborne Rotating Lidar Instrument Experiment. Preprints, *19th Int. Laser Radar Conf.*, NASA/CP-1998-207671/PT2, Annapolis, MD, NASA, 623–626.
- Simpson, J. E., 1987: *Density Currents in the Environment and the Laboratory*. 2nd ed. Cambridge University Press, 244 pp.
- Smith, R. K., 1988: Travelling waves and bores in the lower atmosphere: The “Morning Glory” and related phenomena. *Earth-Sci. Rev.*, **25**, 267–270.
- Weckwerth, T. M., and D. B. Parsons, 2006: A review of convection initiation and motivation for IHOP_2002. *Mon. Wea. Rev.*, **134**, 5–22.
- , and Coauthors, 2004: An overview of the International H₂O Project (IHOP_2002) and some preliminary highlights. *Bull. Amer. Meteor. Soc.*, **85**, 253–277.
- Whiteman, D. N., and Coauthors, 2006: Raman lidar measurements during the International H₂O Project. Part I: Instrumentation and analysis techniques. *J. Atmos. Oceanic Technol.*, **23**, 157–169.
- Xue, M., and W. J. Martin, 2006: A high-resolution modeling study of the 24 May 2002 case during IHOP. Part I: Numerical simulation and general evolution of the dryline and convection. *Mon. Wea. Rev.*, **134**, 149–171.
- , K. K. Droegemeier, and V. Wong, 2000: The Advanced Regional Prediction System (ARPS)— A multi-scale nonhydrostatic atmospheric simulation and prediction model. Part I: Model dynamics and verification. *Meteor. Atmos. Phys.*, **75**, 161–193.
- , and Coauthors, 2001: The Advanced Regional Prediction System (ARPS)— A multi-scale nonhydrostatic atmospheric simulation and prediction model. Part II: Model physics and applications. *Meteor. Atmos. Phys.*, **76**, 145–165.
- , K. Brewster, D. Weber, K. W. Thomas, F. Kong, and E. Kemp, 2002: Realtime storm-scale forecast support for IHOP 2002 at CAPS. Preprints, *15th Conf. on Numerical Weather Prediction/19th Conf. on Weather Analysis and Forecasting*, San Antonio, TX, Amer. Meteor. Soc., 124–126.
- , D. Wang, J. Gao, K. Brewster, and K. K. Droegemeier, 2003: The Advanced Regional Prediction System (ARPS), storm-scale numerical weather prediction and data assimilation. *Meteor. Atmos. Phys.*, **82**, 139–170.